Variations of cyclotron resonant scattering features in Vela X-1 revealed with Insight-HXMT

Q. Liu,[1,2] W. Wang,[1,2]★ Y. Z. Ding,[1,2] X. Chen,[1,2] L. D. Kong,[3] M. Y. Ge,[3] Y. L. Tuo,[3] F. J. Lu,[3] J. L. Qu,[3] S. Zhang[3], and S. N. Zhang[3]
[1]*School of Physics and Technology, Wuhan University, Wuhan 430072, China*
[2]*WHU-NAOC Joint Center for Astronomy, Wuhan University, Wuhan 430072, China*
[3]*Key Laboratory of Particle Astrophysics, Institute of High Energy Physics, Chinese Academy of Sciences, Beijing 100049, China*

9 October 2021

ABSTRACT

We study the variation of cyclotron resonance scattering features (CRSF) in eclipsing high-mass X-ray binary Vela X-1 based on Insight-HXMT observations in 2019 and 2020. We investigate the correlation between cyclotron lines and continuum parameters like photon index and flux. In this analysis, we found that the first harmonic line energy of Vela X-1 varies between ∼43 and ∼52 keV in our phase-averaged spectra. The fundamental line energy is detected at ∼25 keV but is not always clear and it shows a potential increase with time. And in our energy spectrum fitting, we present the relations for two cyclotron line energies and depths respectively, which illustrate that the depth of two lines has a positive correlation. We show you the correlation between depth and photon index, as well as the flux and parameters such as photon index and cyclotron line centroid energy. The depth with photon index has a positive correlation but the photon index show a negative correlation with energy flux. Both two line energies show no evident correlation with flux. Then we performed a pulse phase resolved spectroscopy in Vela X-1, all of harmonic cyclotron lines can be confirmed. But the fundamental CRSFs is mainly detected in the main and secondary pulses and it is far less detected during the pulse minimum. In the phase resolved resulting, we obtain the evolution of cyclotron lines and continuum with flux. In the end, we discuss the underlying physics accretion process in highly magnetized neutron stars. These results may contribute to the interpretation of geometrical structure of the line forming region.

Key words: stars: neutron - pulsars: individual: Vela X-1 - X-rays: binaries - stars: magnetic field

1 INTRODUCTION

Vela X-1 is a wind-accreting and an eclipsing high-mass neutron star X-ray binary consisting of a neutron star of ∼ $1.77 M_{\odot}$ (Rawls et al. 2011) which its period is ∼ 283s (McClintock et al. 1976) with an 8.964d (van Kerkwijk et al. 1995) orbit rotating around B0.5Ib super-giant HD 77523 (Hiltner et al. 1972). The system is at a distance 1.9 ± 0.2 kpc (Sadakane et al. 1985) and its separation of the binary system is just 1.7 $R_{\star}$ (Quaintrell et al. 2003) (orbital radius). The early type optical companion has a mass of ∼23 $M_{\odot}$ and a radius of ∼30 $R_{\odot}$ (van Kerkwijk et al. 1995). The neutron star is the most massive compact object up to now and is deeply embedded in the dense stellar wind. The flux is strongly variable and its X-ray luminosity is typically $5{\times}10^{36}$erg s^{-1} (Fürst et al. 2010).

Cyclotron resonant scattering features (CRSFs) are an identified characteristic absorption in the X-ray spectra. The magnetic fields on surface of neutron stars can be directly measured by the absorption lines. The electrons perpendicular to the strong magnetic fields can be quantized into discrete Landau levels (Schönherr et al. 2007), and photons with energies close to these levels produce an absorption characteristics in their spectra by scattering off these electrons. The magnetic field intense can be calculated by

$$B = \frac{E_n}{n \times 11.57\mathrm{keV}} \times 10^{12}\mathrm{G} \quad (1)$$

where E_n is the cyclotron line energy in keV, the fundamental line (n = 1) and harmonic line (n = 2).

The first detection for the first harmonic near 50 keV was found by Kendziorra et al. (1992) in Vela X-1. But it is not the fundamental line and the lower line energy of Vela X-1 is barely detectable. Makishima & Mihara (1992) and Choi et al. (1996) reported an absorption line feature at ∼32 keV with Ginga data. The confirmation of two line features around ∼23 keV and ∼45 keV have been reported by Kretschmar et al. (1997) using the data from HEXE. In recent years, Maitra & Paul (2013) and Odaka et al. (2013) reported the detection of CRSFs at ∼25 and 50 keV with Suzaku observational data. And Wang (2014) confirmed CRSFs at about 25 and 55 keV in the hard X-ray spectra of Vela X-1 by INTEGRAL. Fürst et al. (2014) shows the anti-correlated between the depths of the two lines and they thought this result deriving from photon spawning (Schönherr et al. 2007). Many observations like Klochkov et al. (2012) studied the correlation between CRSFs and flux in accreting X-ray pulsars. These researches can help to understand the accretion geometry or physical processes onto the magnetic poles of strongly magnetized neutron star surface in a wind-accreting X-ray binaries. And we would like to study the properties of Vela X-1 in detail and search for cyclotron lines in the hard X-ray spectra in range of 2-105 keV, and study their variation and correlation with long-term data as observed by Insight-HXMT.

Further more, the CRSF parameters over different pulse phase can provide vital information on the magnetic field structure of the

★ E-mail: wangwei2017@whu.edu.cn

emission region on neutron star. Mihara (1995) reported that the CRSFs vary in strength in different phase of the orbit with Ginga. Kreykenbohm et al. (1999) also supported the existence of the two lines using Rossi X-ray Timing Explorer (RXTE) data and found it's variation with the pulse phase in the phase resolved analysis. La Barbera et al. (2003) confirmed the presence at ~55 keV in Vela X-1 with phase resolved analysis performed based on BeppoSAX data. In order to study spectra properties at different viewing angles with pulse, here we also introduce phase phased resolved spectroscopy in Vela X-1.

The paper is structured as follows. Section 2 briefly describes the HXMT observations and data reduction. Section 3 studies the phase averaged X-ray spectrum of Vela X-1 and analyzes the variations and correlations. We present a phase-resolved spectroscopy analysis in Section 4. Section 5 gives the summary.

2 OBSERVATIONS AND DATA REDUCTION

The Hard X-ray Modulation Telescope (HXMT) (Zhang et al. 2020) launched on 15th June 2017, is the first X-ray astronomical satellite in china, which consists of three instruments with a total energy band in 1–250 keV : High Energy X-ray telescope (HE) from 20 to 250 keV band with detector areas of ~5100 cm^2, Medium Energy X-ray telescope (ME) for 5–30 keV band having areas of 952 cm^2, and Low Energy X-ray telescope (LE) for 1–15 keV band with a total area of 384cm^2.

The HE contains 18 NaI(Tl)/CsI(Na) scintillation detectors, which include 15 narrow FOV($5.7^\circ \times 1.1^\circ$), 2 wide FOV($5.7^\circ \times 5.7^\circ$) and a blind FOV. Both of ME and LE X-ray telescope consist of three detector boxes. For each detector box of ME has 576 Si-PIN detector pixels. For each detector box of LE contains 32 CCD236 (a kind of Swept Charge Devices).

The Insight-HXMT Data Analysis Software (HXMTDAS) v2.04 is used for data analysis. We require the good time intervals (GTIs) in HXMTDAS using hegtigen, megtigen, and legtigen tasks which all adopt the pointing offset angle $< 0.04^\circ$, the elevation angle $> 10^\circ$, and the geomagnetic cut-off rigidity >8 GV. Background light curves are estimated by making use of hebkgmap, mebkgmap and lebkgmap tasks. Tasks helcgen, melcgen and lelcgen are used to generate light curve with 0.078125 sec time bins.

We use the 11 observations in 2020 and one observation in 2019 to study Vela X-1 in phase averaged spectra. For phase resolved analysis, we choose the exposure number P020101214909 due to higher strength in cyclotron lines. We divide pulse phase by 16 bins and generate new spectra, background and response matrix for each time bin with HXMTDAS. We used XSPEC 12.11.1 (Arnaud 1996) with several custom models for the spectral analysis.

3 PHASE AVERAGED SPECTRAL ANALYSIS

The formed shape of the continuum spectra is believed to be dominated by the emission of Comptonization of thermal photons. For Compton scattering (Sturner & Dermer 1994; Alexander et al. 1996) continuum spectrum, Here we continue to select empirical models which is a analytic power law at low energies with exponential cutoff function at higher energies (White et al. 1983; Tanaka 1986) to model the spectral continua of accreting X-ray pulsars for data analysis.

To test the model of the continuum emission of Vela X-1, a simple power law with high energy exponential rolloff (cutoffpl) does not fit the data fine. We use a powerlaw continuum with a Fermi-Dirac cut-off (FDcut) (Tanaka 1986). The FDcut function is parameterized by the photon index Γ, the cutoff energy E_{cut} ,and the folding energy E_{fold} in the following expression

$$F(E) \propto E^{-\Gamma} \times \left(1 + \exp\left(\frac{E - E_{\rm cut}}{E_{\rm fold}}\right)\right)^{-1} \quad (2)$$

The cyclotron scattering line component is well described with a Lorentzian profile model (cyclabs in XSPEC).

$$M(E) = \exp\left[-D_{\rm f}\frac{\left(W_{\rm f}E/E_{\rm cyc}\right)^2}{\left(E - E_{\rm cyc}\right)^2 + W_{\rm f}^2}\right] \quad (3)$$

where $D_{\rm f}$ represents the depth of the line, $W_{\rm f}$ describe the width of the line, and $E_{\rm cyc}$ is the centroid cyclotron line energy.

Vela X-1 sometimes shows emitting lines associated with Fe Kα in its soft X-ray spectrum. We described these lines with a Gaussian function around 6.4 keV. In order to describe the hydrogen column absorption, we adopt phabs (XSPEC) model. To allow the cross-calibration difference being below 5% in different payloads, we add a relative normalization constant in the model. Finally we performed a phase averaged spectral fitting.

3.1 Cyclotron line energies

Here we show spectrum fitting results. In Fig. 1, we present the hard X-ray spectrum fitting from 2–105 keV for Vela X-1. The spectrum is first fitted with a FD-cut multiplied by phabs(XSPEC) model in Fig. 1 (a). There exists obvious absorption lines in the spectrum. In Fig. 1 (b), a cyclotron resonant scattering line component around 45 keV is added into the spectral fitting. There still is an absorption-line feature around 23 keV (he fundamental line). We add the line in Fig. 1 (c). The Fe Kα line about 6.4 keV is fitted in Fig. 1 (d).

In Table 1, the parameters of fitting spectrum in four models mentioned above are displayed. The first harmonic line in Vela X-1 is determined to be at ~46 keV. In addition, the fundamental line can be fitted very well at ~26keV. Comparing the two cyclotron line features, it is obvious that the fundamental line is always narrower and shallower than that of the first harmonic in Vela X-1. The fitting Fe Kα line energy is about 6.5KeV, and the width can be determined to be 0.13keV which looks broaden.

Segreto et al. (2010) found that the first harmonic of Vela X-1 exist a decrease by ~0.72 keV per year in 2004 till 2010 using Swift/BAT data and then remain a constant. We have also investigated the evolution of cyclotron line energy with time. The upper plot in Fig. 2 is the first harmonic line and lower plot is the fundamental line. We found that the first harmonic line energy varying between ~43 and~52 keV in Vela X-1 is close to a quite stable constant in our phase-averaged analysis which is consistent with Segreto et al. (2010). On the contrary, the fundamental line energy may have a potential increase due to limited statistics. Staubert et al. (2014, 2016) reported in Her X-1 the fundamental CRSF energy reduce by 5 keV from 1996 to 2015 with the data obtained with RXTE, Beppo-SAX, INTEGRAL, Suzaku and NuSTAR. More interestingly, Staubert et al. (2017) recently announced that the 20 years's decrease has stopped and have an inverse trend. In this paper, our results of Vela X-1 seems to be a semblable trend as Her X-1.

The physical mechanism of the long-term variation of CRSFs energy is no such a straightforward explanation. It is possible that the magnetic field at the polar cap have changed. We tend to that it is due to the resonant scattering of photon lie in different regions of the accretion column surface.

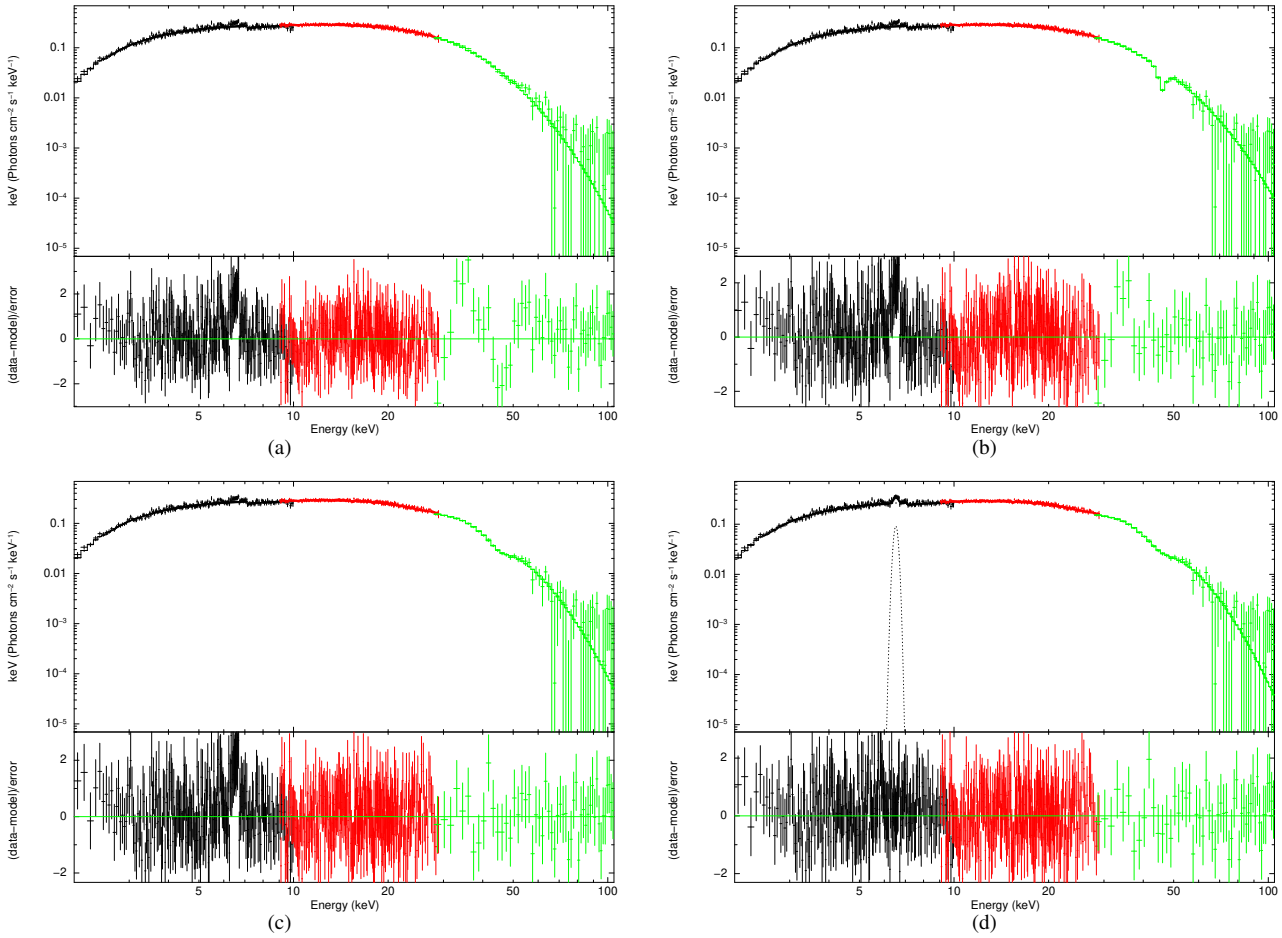

Figure 1. The hard X-ray spectrum from 2–105 keV of Vela X-1 obtained by Insight-HXMT. (a) The spectrum is fitted with a FD-cut multiplied by phabs(XSPEC) model. (b) The spectrum is fitted with a FD-cut multiplied by phabs(XSPEC) plus a cyclotron scattering line around 45 keV. (c) The spectrum is fitted with a FD-cut multiplied by phabs(XSPEC) plus two cyclotron scattering lines at ~23 and 45 keV. (d) The spectrum is fitted with a FD-cut multiplied by phabs(XSPEC) plus two cyclotron scattering lines at ~23 and 45 keV with an Fe Kα line at 6.4 keV.

Table 1. The best-fitting spectral parameters of Vela X-1 in three different luminosity ranges in the hard X-ray bands from 3–200 keV discussed in Section 3.1. (1) FD-cut and phabs model phabs*FD-cut; (2) FD-cut multiplied by phabs(XSPEC) plus a cyclotron scattering line phabs*FD-cut*cyclabs; (3) FD-cut multiplied by phabs(XSPEC) plus two cyclotron scattering lines phabs*FD-cut*cyclabs*cyclabs; (4) FD-cut multiplied by phabs(XSPEC plus two cyclotron scattering lines, with an Fe Kα line around 6.4 keV; The continuum flux is given in units of 10^{-9} erg cm^{-2} s^{-1}.

Model	nH	Γ	E_{cutoff}	E_1	$Width_1$	$Depth_1$	E_2	$Width_2$	$Depth_2$	Flux	χ^2
1	$2.03^{+0.14}_{-0.15}$	$0.95^{+0.03}_{-0.03}$	$25.75^{+1.04}_{-0.75}$							$7.503^{+0.065}_{-0.036}$	1.031
2	$1.93^{+0.13}_{-0.13}$	$0.91^{+0.03}_{-0.04}$	$24.21^{+0.63}_{-1.22}$				$46.89^{+1.5}_{-1.31}$	$1.04^{+0.5}_{-0.02}$	$1.31^{+0.48}_{-0.5}$	$7.655^{+0.06}_{-0.07}$	1.009
3	$2.06^{+0.08}_{-0.11}$	$0.97^{+0.02}_{-0.04}$	$30.04^{+1.55}_{-2.03}$	$26.69^{+0.32}_{-1.27}$	$3.68^{+2.65}_{-1.03}$	$0.23^{+0.05}_{-0.1}$	$45.76^{+0.82}_{-0.37}$	$12.56^{+3.86}_{-6.24}$	$0.77^{+0.23}_{-0.24}$	$7.402^{+0.152}_{-0.026}$	0.986
4	$2.03^{0.12}_{-0.03}$	$0.99^{0.03}_{-0.01}$	$29.81^{2.43}_{-1.05}$	$26.78^{+0.88}_{-0.61}$	$3.91^{+3.08}_{-0.83}$	$0.22^{+0.0}_{-0.08}$	$45.28^{+2.66}_{-1.67}$	$9.35^{+3.54}_{-3.2}$	$0.62^{+0.31}_{-0.21}$	$7.4^{+0.141}_{-0.046}$	0.879

3.2 Correlation

We show the correlation for two CRSFs line energy or depth. In Fig. 3, we find that there exist no evident relation between the first harmonic line energy and the fundamental. But the depth between the two lines gives the positive correlation in Fig. 4. We think it is a natural phenomenon that strength of both of two line became much stronger with intensive scatter interaction.

The two CRSFs line energy versus the photon index are shown in Fig. 5, E_2 and E_1 has no relation to the X-ray photon index. In the contrast, both of the depth of the two cyclotron features show a increase with the photon index as seen in Fig. 6. Here show you the correlation between photon index and flux in Fig. 7. Our results show there may be exist a negative relation between the photon index and flux.

Fürst et al. (2014) reported the energy increase of the harmonic line with luminosity. La Parola et al. (2016) also proposed the positive correlation between the harmonic line energy and luminosity with

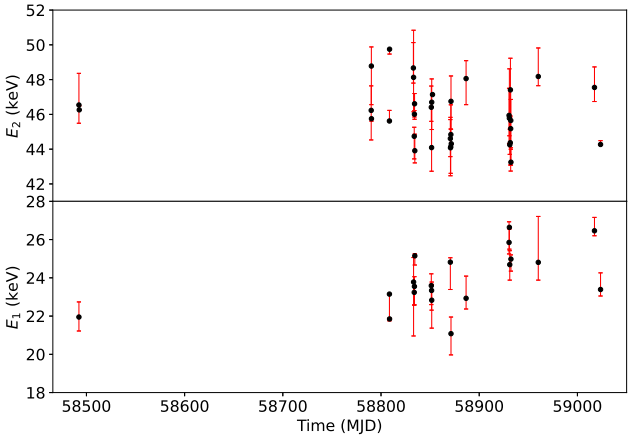

Figure 2. The evolution of cyclotron line energy with time studied in Section 3.1. The upper plot is the first harmonic line and lower plot is the fundamental line.

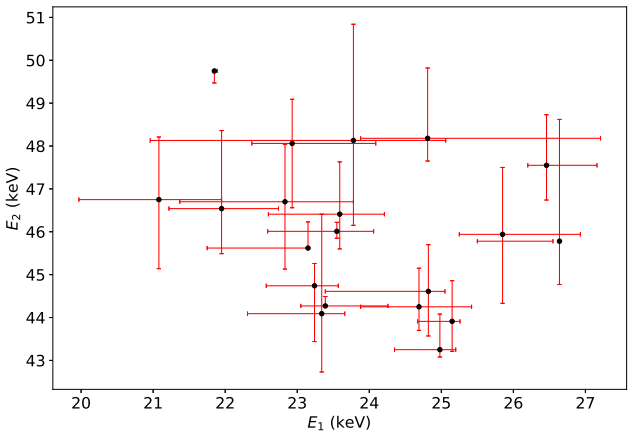

Figure 3. The correlation between the first harmonic line energy and the fundamental.

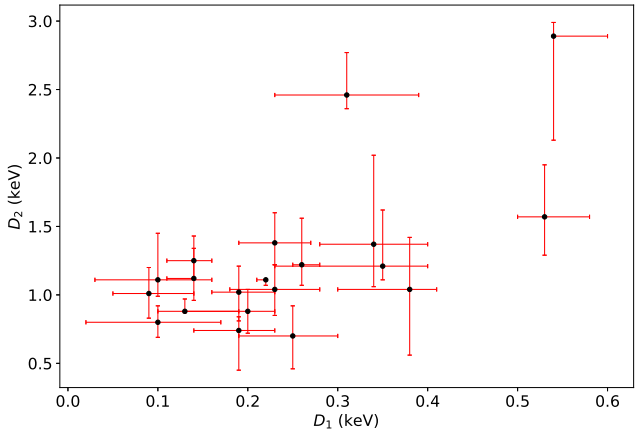

Figure 4. The correlation between the first harmonic line depth and the fundamental.

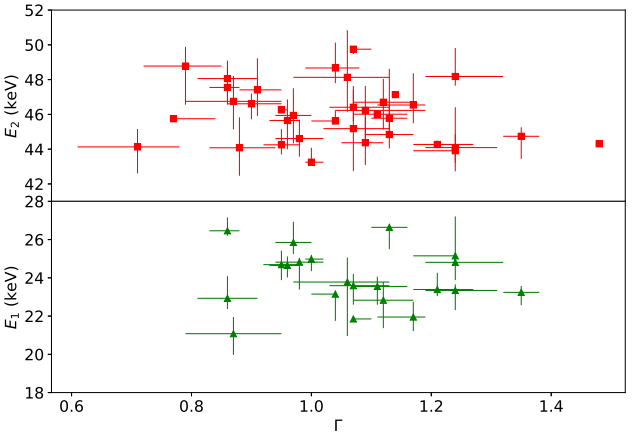

Figure 5. The correlation between the line energy and photon index. The upper plot is the first harmonic line and lower plot is the fundamental line.

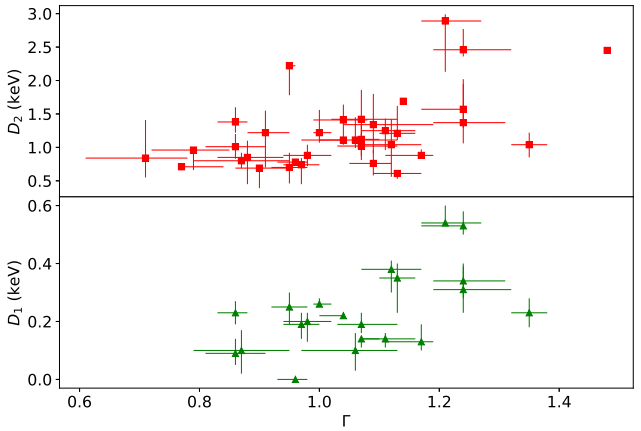

Figure 6. The correlation between the line width and photon index. The upper plot is the first harmonic line and lower plot is the fundamental line.

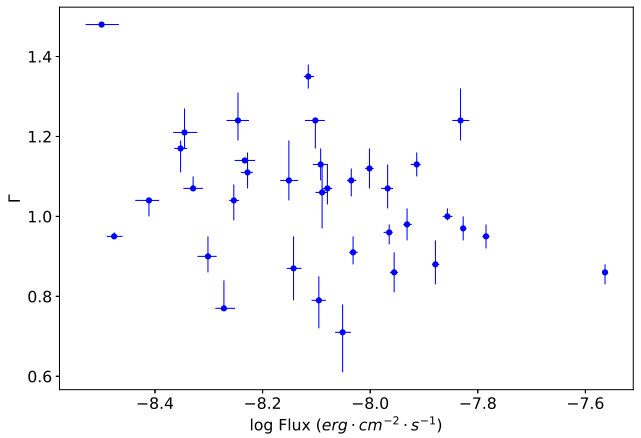

Figure 7. The correlation between photon index and flux.

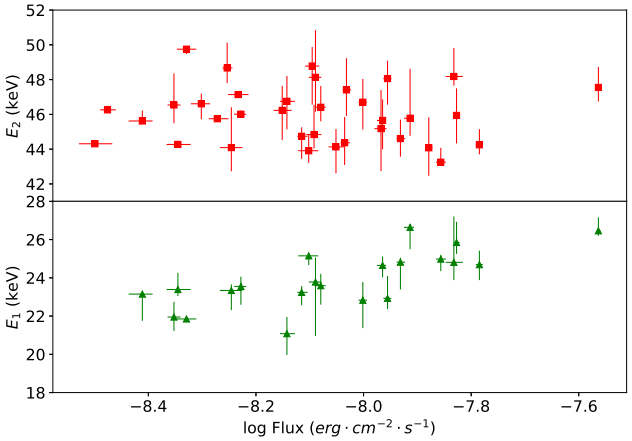

Figure 8. The correlation between the line energy and flux. The upper plot is the first harmonic line and lower plot is the fundamental line.

an a long-term data for Swift/BAT. In Fig. 8, the first harmonic line energy we obtained have no visible relation with flux, but we found the fundamental line seem to be positive correlation with flux. This a new discovery because the fundamental line is not always detectable.

4 PHASE RESOLVED SPECTROSCOPY

The spectra observed has been found to vary in different pulse phases due to the viewing angle with respect to the scattering region. This variations can be used to infer accretion process of the emission region and geometric characteristic.

The pulse profile for the accreting pulsar is usually highly energy dependent. Energy resolved pulse profiles were created by folding the light curves in different energy bands with the obtained pulse period as seen Fig. 9. Strong energy dependence of the pulse profiles implies dependence of the energy spectrum on the flux. Above 10 keV, the pulse profile consists of two peaks which are about equally strong. We designate the first pulse as the secondary pulse and the second as main pulse.

Below 10 keV, these two pulses evolve into multi-peaks. The pulse profiles exhibit both intensity and energy dependence with multiple peaks at low energies and double peaks at higher energies.

To investigate this in detail, we present a detailed pulse phase resolved spectral analysis of the persistent high mass X-ray binary pulsar Vela X-1 observed with Insight-HXMT. After barycentering and orbital motion correction of Vela X-1 using the ephemeris (Nagase 1989), we divided the phase for 16 overlapping bins using the derived pulse periods of P = 283.5s at MJD 58931.1087. For every phase resolved spectrum we regenerate the new background spectra and response matrices using HXMT software. We fitted the spectra the same as in phase averaged case.

4.1 The cyclotron parameters

Fig. 10 shows that the variation of the cyclotron parameters for line forming region as a function of pulse phase profile. The CRSFs energy change with the pulse phase which may contribute to constrain the accretion column geometry in regard to rotation axis of the neutron star under different viewing angle. In particular, the strength (depth) of the cyclotron line also depends highly on pulse phase. But the fundamental line is not always seen at all of pulse phases

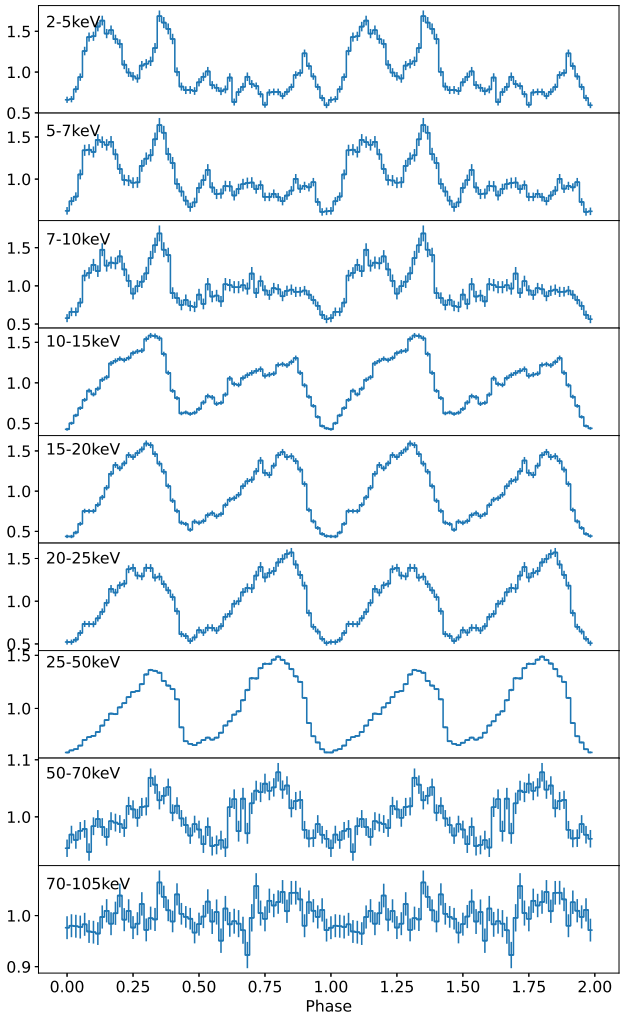

Figure 9. The pulse profile in different energy range.

(Kreykenbohm et al. 2002). Further more, the correlation of energy and depth for the fundamental CRSFs is positive which illustrate the fundamental line depth is much larger with the increasing corresponding energy. This characteristics could imply that the emission pattern vary on the pulse phase so that the fundamental CRSFs is very shallow or not always present.

4.2 The continuum parameters

Fig. 10 shows the best-fit phase resolved continuum parameters as a function of the pulse phase. They usually vary smoothly sometimes shrilly. The photon index Γ and the hydrogen column N_H in low energy absorption changed by the variance of $\sim$ 1. and $\sim$ 4 in units of 10^{22} atoms cm^{-2} respectively. Both of them has a prominent double peaks structures and exists a phase lag in the evolution. We found that the cut off energy E_c have a good agreement with pulse phase. The fold energy E_f also show a variation with phase as these similar changes can be seen on timescales.

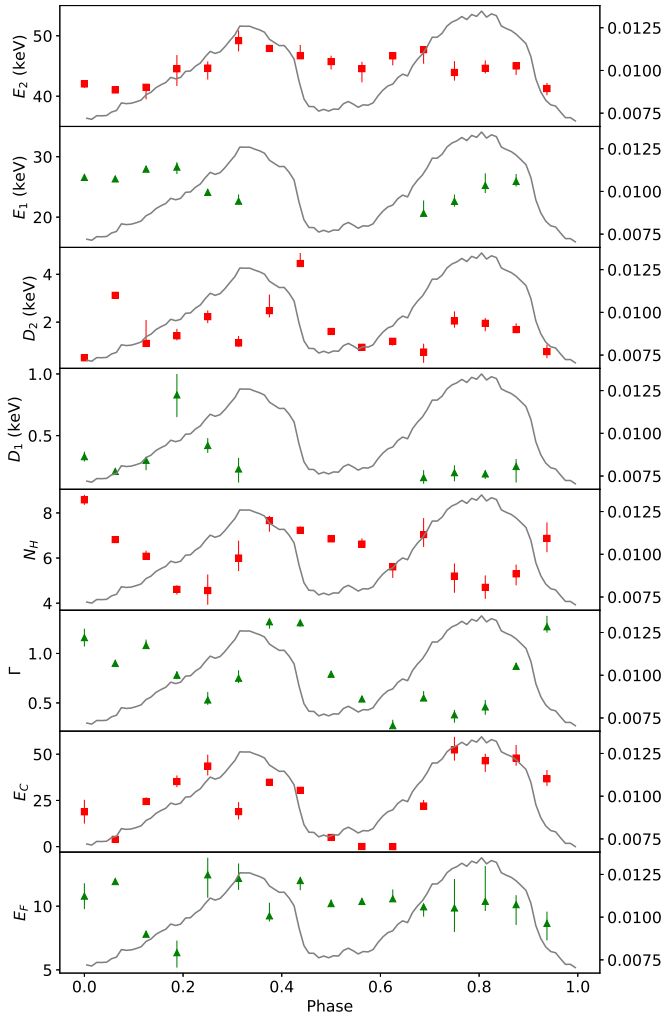

Figure 10. The evolution of fit cyclotron parameters over the phase pulse and the continuum parameters over the phase pulse in phase resolved spectroscopy. E2 is the energy of the CRSF at ~45 keV and D2 its depth. E1 is the energy at ~25 keV and D1 its depth.

5 SUMMARY AND DISCUSSION

We investigated the evolution of centroid energy of cyclotron lines, and found that the first harmonic line energy varying between ~43 and ~52 keV in Vela X-1 approximately remain a constant. On the contrary, the fundamental line energy has a weak increase. In energy spectrum fitting, the two cyclotron lines depth have a increase with the photon index. The fundamental line energy show a positive correlation with energy flux. After performing a pulse-phase resolved spectroscopy, the cyclotron parameters as a function of pulse can be presented. The harmonic energy has a evident evolution with phase. It could indicate that the magnetic field configuration in emitting region of cap polar are different. The fundamental line energy also change by pulse phase and is roughly consistent with the depth. The ratio of energy for two line rise up with phase in secondary pulse and decline in main pulse as shown in Fig. 11. These results imply possible radiation process in the polar cap region or accretion geometrical structure and will make more discussions.

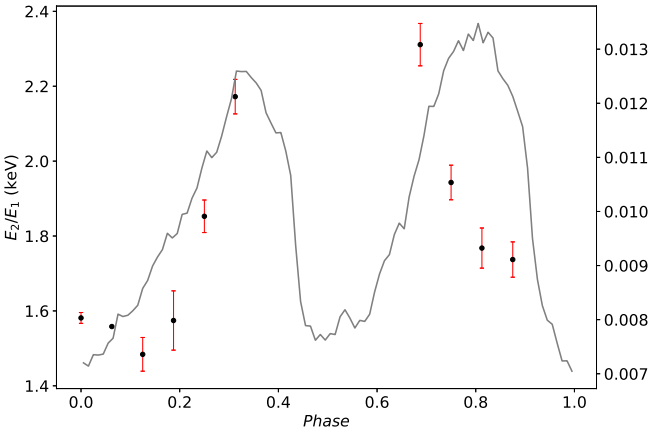

Figure 11. The ration of two CRSFs energy versus phase

ACKNOWLEDGEMENTS

The work is supported by the NSFC (12133007, U1838103, 11622326, U1838201, U1838202). This work made use of data from the *Insight*-HXMT mission, a project funded by China National Space Administration (CNSA) and the Chinese Academy of Sciences (CAS).

DATA AVAILABILITY

Data that were used in this paper are from Institute of High Energy Physics Chinese Academy of Sciences(IHEP-CAS) and are publicly available for download from the *Insight*-HXMT website. To process and fit the spectrum and obtain folded light curves, this research has made use of XRONOS and FTOOLS provided by NASA.

REFERENCES

Alexander S. G., Davila J., Dimattio D. J., 1996, ApJ, 459, 666
Arnaud K. A., 1996, in Jacoby G. H., Barnes J., eds, Astronomical Society of the Pacific Conference Series Vol. 101, Astronomical Data Analysis Software and Systems V. p. 17
Choi C. S., Dotani T., Day C. S. R., Nagase F., 1996, ApJ, 471, 447
Fürst F., et al., 2010, A&A, 519, A37
Fürst F., et al., 2014, ApJ, 780, 133
Hiltner W. A., Werner J., Osmer P., 1972, ApJ, 175, L19
Kendziorra E., et al., 1992, in Tanaka Y., Koyama K., eds, Frontiers Science Series. p. 51
Klochkov D., et al., 2012, A&A, 542, L28
Kretschmar P., et al., 1997, A&A, 325, 623
Kreykenbohm I., Kretschmar P., Wilms J., Staubert R., Kendziorra E., Gruber D. E., Heindl W. A., Rothschild R. E., 1999, A&A, 341, 141
Kreykenbohm I., Coburn W., Wilms J., Kretschmar P., Staubert R., Heindl W. A., Rothschild R. E., 2002, A&A, 395, 129
La Barbera A., Santangelo A., Orlandini M., Segreto A., 2003, A&A, 400, 993
La Parola V., Cusumano G., Segreto A., D'Aì A., 2016, MNRAS, 463, 185
Maitra C., Paul B., 2013, ApJ, 763, 79
Makishima K., Mihara T., 1992, in Tanaka Y., Koyama K., eds, Frontiers Science Series. p. 23
McClintock J. E., et al., 1976, ApJ, 206, L99
Mihara T., 1995, Ph.D. Thesis
Nagase F., 1989, PASJ, 41, 1
Odaka H., Khangulyan D., Tanaka Y. T., Watanabe S., Takahashi T., Makishima K., 2013, ApJ, 767, 70

Quaintrell H., Norton A. J., Ash T. D. C., Roche P., Willems B., Bedding T. R., Baldry I. K., Fender R. P., 2003, A&A, 401, 313
Rawls M. L., Orosz J. A., McClintock J. E., Torres M. A. P., Bailyn C. D., Buxton M. M., 2011, ApJ, 730, 25
Sadakane K., Hirata R., Jugaku J., Kondo Y., Matsuoka M., Tanaka Y., Hammerschlag-Hensberge G., 1985, ApJ, 288, 284
Schönherr G., Wilms J., Kretschmar P., Kreykenbohm I., Santangelo A., Rothschild R. E., Coburn W., Staubert R., 2007, A&A, 472, 353
Segreto A., Cusumano G., Ferrigno C., La Parola V., Mangano V., Mineo T., Romano P., 2010, A&A, 510, A47
Staubert R., Klochkov D., Wilms J., Postnov K., Shakura N. I., Rothschild R. E., Fürst F., Harrison F. A., 2014, A&A, 572, A119
Staubert R., Klochkov D., Vybornov V., Wilms J., Harrison F. A., 2016, A&A, 590, A91
Staubert R., Klochkov D., Fürst F., Wilms J., Rothschild R. E., Harrison F., 2017, A&A, 606, L13
Sturner S. J., Dermer C. D., 1994, A&A, 284, 161
Tanaka Y., 1986, Observations of Compact X-Ray Sources. p. 198, doi:10.1007/3-540-16764-1_12
Wang W., 2014, MNRAS, 440, 1114
White N. E., Swank J. H., Holt S. S., 1983, ApJ, 270, 711
Zhang S.-N., et al., 2020, Science China Physics, Mechanics, and Astronomy, 63, 249502
van Kerkwijk M. H., van Paradijs J., Zuiderwijk E. J., Hammerschlag-Hensberge G., Kaper L., Sterken C., 1995, A&A, 303, 483